RSC Advances

ROYAL SOCIETY OF CHEMISTRY

www.rsc.org/advances

RSC Advances

ARTICLE

Thin Carbon Layer Coated Multiwalled Carbon Nanotube Composite Electrodes for Supercapacitors

Sung-Kon Kim[a] and Ho Seok Park[b,*]

Submicron thin films of composite (CSN) electrodes are prepared by a simple spin-coating of multiwalled carbon nanotube (MWNT) suspension with sucrose as a precursor for thin carbon layer, followed by heat treatment at 1000 ^{o}C for 2 h. Thin carbon layers are coated on the outer surface of MWNT and the resulting CSN electrode is shown to be interconnected open network structure. The binder-free thin film CSN electrode having such unique architecture shows large areal capacitance of ~723 μF cm^{-2} at a constant current of 0.23 μA cm^{-2} in a Na$_2$SO$_4$ aqueous electrolyte and preserves ~81% of its initial capacitance even at high specific current value. According to the results of electrochemical impedance spectroscopy, the CSN electrode can concurrently optimize ion and electron transport for high power delivery. It also exhibits good cycle stability after prolonged operation (up to 3000 charging/discharging cycles).

1. Introduction

Electric energy storage (EES) is a key technology to current growing needs for fast developments of portable electronics, smart grid, and hybrid electric vehicles.[1] Over the past decades, supercapacitors (SCs), also known as electrochemical capacitors or ultracapacitors, have gained significant attention as an emerging candidate for smart and efficient EESs due to high power capability, nearly infinite cycle life, safe operation for ~10 years, and low manufacturing cost.[2-6] An ideal approach to high-performance SC is to improve surface area and electrical conductivity of electrodes in which charges are stored at the electrolyte/electrode interfaces while forming electrical double layers.[7, 8] Nanostructured carbon materials, such as carbon nanotubes (CNTs),[9] graphene,[4] carbide-derived carbon,[10, 11] and onion-like carbon,[12] are featured by high surface area, high electrical conductivity, and good chemical inertness, and thus they have been particularly explored as electrode materials for SCs. However, some of them still undergo significant capacitance drop because of the loss of ion-accessible surface area during the process of assembling the nanoscale building block into macroscopic structures.[13] For examples, the CNT-based electrodes show good electrical conductivity and large ion-accessible surface area, but their capacity is limited because the charges transport is restricted by a variety of boundaries in the CNT network format.[14-16] In addition, graphene, another excellent electrode material, suffer from irreversible agglomeration and substantial restacking of the individual sheets during the electrode consolidation owing to the strong π – π stacking and van der Waals force between the planar basal planes of graphene sheets, leading to great loss of effective surface area and consequently lower specific capacitance.[13, 17] Thus, the development of new electrode materials with high performance still remains challenging.

Considerable research efforts on the design and fabrication of composite electrode materials based on CNTs such as graphene/CNT,[18-20] metal oxide/CNT,[21, 22] and conducting polymer/CNT[23] have been devoted due to their high electrical conductivity with unique tubular structures and a large ion-accessible surface area that can provide good rate capability. The SCs using the composite electrodes deliver excellent power densities and store more energy than conventional energy storage devices. Here, we report a composite electrode consisting of multiwalled carbon nanotube (MWNT) and sucrose-derived carbon (CS) with highly accessible surface area and high electrical conductivity by simple spin-coating and subsequent carbonization. It shows highly ion-accessible open structure and good electrical conductivity. The resulting SC using the composite electrode exhibits a large areal capacitance (723 μF cm^{-2}), fast rate capability, and good cycle stability up to 3000 cycles at a constant current.

2. Experimental

2.1 Preparation of SC electrodes

1.25 g of sucrose ($\geq$99.5%, Aldrich), 0.14 g of H$_2$SO$_4$ (95-97%, Fluka), 5.0 mL of deionized water, and 1.66 g of MWNT suspension (3 wt% in water, Nanostructure & Amorphous Materials, Inc.) were mixed and then sonicated for 2 h. The silicon wafer with double side SiO$_2$ layers were treated by oxygen plasma using 300 W for 5 min to make it hydrophilic, and then as-prepared suspension mixture was spin-coated (2000 rpm, 60 s) on the silicon wafer substrate two times. The produced mixture films were heated to 1000 ^{o}C with a ramping rate of 20 ^{o}C min^{-1} in a tubular furnace under 5% H$_2$ and 95% Ar gas and then temperature was kept at the same temperature for 2 h. The resulting black thin film was washed with copious Millipore water and then was dry under gentle nitrogen stream.

For comparison, CS film was prepared under same conditions without adding MWNT. MWNT film was fabricated by a spin-coating of MWNT suspension two times. Annealed MWNT (aMWNT) film was prepared by taking a subsequent heat treatment of the MWNT film at 1000 ^{o}C for 2 h under 5% H$_2$ and 95% Ar gas.

2.2 Characterization

Oxygen plasma treatment was performed in a March RIE CS-1701. The microstructures were imaged using Hitachi S-4700 SEM and JEOL 2100 TEM. Raman spectroscopic measurement was performed with Raman-11 (Nanophoton, Japan) using a 532 nm laser source. The chemical structure was determined by X-ray photoelectron spectroscopy (XPS, Axis Ultra, Kratos Analytical). Electrochemical characterization, including cyclic voltammetry (CV), galvanostatic charge/discharge (GCD), and electrochemical impedance spectroscopy (EIS), was performed using a VMP3 multichannel potentiostat (Bio-Logic, USA) in the two-electrode mode at room temperature. In the GCD profiles, the areal capacitance can be estimated using the following equation:

$$C = 2I/[(\Delta V/\Delta t)A] \quad (1)$$

where I is the current applied, $\Delta V/\Delta t$ is the slope of the discharge curve after IR drop at the beginning of the discharge curve, and A is the area of electrodes (in cm^2).

3. Results and discussion

The thin carbon layer coated multiwalled carbon nanotube composite, abbreviated as CSN, electrode was fabricated by a straightforward spin-coating method using a mixture of sucrose and MWNT suspension on SiO$_2$ thin film-coated silicone substrate, followed by heat treatment at 1000 ^{o}C for 2 h under a slow stream of forming gas (5% H$_2$/ 95% Ar). Sucrose (C$_{12}$H$_{22}$O$_{11}$) is an organic compound, commonly known as a sugar, and can be a carbon material when it is pyrolyzed (Fig. 1).[24] The spin-coated MWNT forms a porous network structure as expected and the structure still remains unchanged even when CS is added into the MWNT (Fig. 2).[25] Unlike spin-coating method, solution-casting of the precursor mixture of CSN gives rise to compact structure with little pores as reported previously (Fig. 2d).[26, 27] MWNTs are almost buried underneath CSs and thus sacrifice their porous texture. In addition to electrical conductivity, the surface area of electrodes plays a key role in determining SC performance and thus such highly packed electrode cannnot guarantee large performance per unit area. In other words, while graphitizing sucrose upon heat treatment, MWNTs serve as a framework to bind CS *via* strong π–π stacking and van der Waals forces between their neighboring surfaces (Fig. 2e,f).[13] CSs are distributed through the entangled MWNT framework to form a conductive interconnected CSN network, which is beneficial for electron transport (Fig. 2f). It is believed that the CSN structure not only
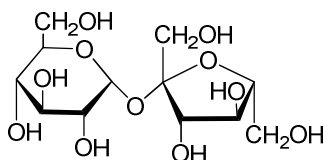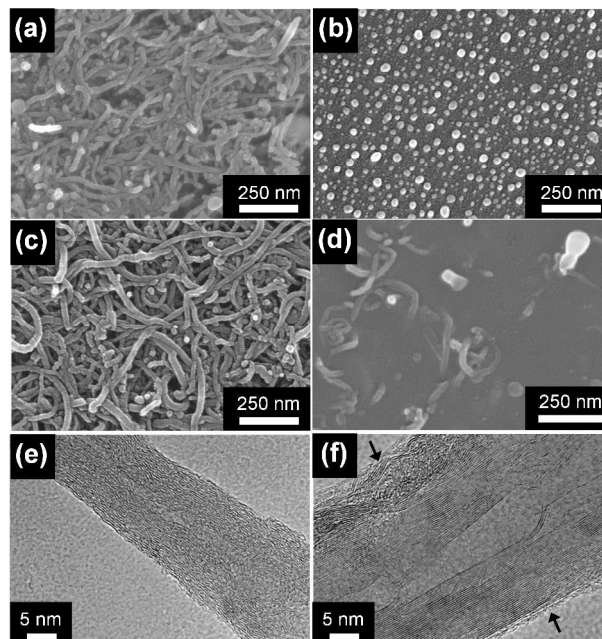

Fig. 2 SEM images of (a) aMWNT, (b) CS, (c) spin-coated CSN, and (d) solution-casted CSN. TEM micrographs of (e) aMWNT and (f) spin-coated CSN (Arrows indicate thin CS layers).

provides high specific surface area of the electrode as it forms open network structure, which is favorable for improving electrochemical capacitance, but also offers ionic transportation channels during the electrochemical charging and discharging process. As a result, binder-free CSN electrode prepared by spin-coating and subsequent thermal treatment provides a continuous MWNT network with irregular porous architecture in which CS is attached onto outer walls of MWNT. This structure can minimize electron transport lengths and ion diffusion distances, which will be discussed in the following section.

Fig. 3 shows the Raman spectra of MWNT, aMWNT, CS, and CSN. Raman spectroscopy is commonly utilized to characterize the graphitization degree of carbon materials.[28] In
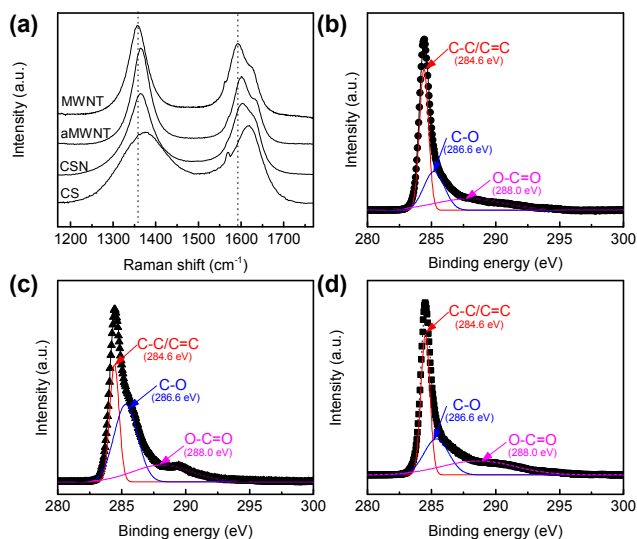

Fig. 3 (a) Raman spectra of MWNT, aMWNT, CS, and CSN. (b) XPS C1s spectra of (b) aMWNT, (c) CS, and (d) CSN.

Fig. 1 Chemical structure of sucrose.

the Raman spectrum of MWNT, two characteristic peaks appear at 1357 and 1592 cm^{-1}, corresponding to D and G peaks, respectively. The D band, associated with the A$_{1g}$ breathing vibration of aromatic six-membered rings, is proportional to the amount of sp^3 carbons in surroundings, whereas the G band results from the E$_{2g}$ in-plane vibrational mode within aromatic carbon rings.[29] Two intense D and G peaks of aMWNT, however, are slightly shifted upward with respect to those of the MWNT and observed at ~1364 and ~1600 cm^{-1}, respectively, both of which are mostly due to disordering on the surface of MWNT.[26, 30] To disperse MWNT in water *via* noncovalent approach, its suspension contains a little amount of impurities such as surfactants and catalyst which could be possibly adsorbed on the MWNT surface and may cause disordering when carbonized.[31] The fact that the intensity of the D band to G band (I_D/I_G) increases from 1.25 for MWNT to 1.41 for aMWNT may be also associated with increased defect sites of aMWNT.[32] The sucrose is completely converted into carbon with nano-crystalline graphitic domains of different size and order when annealed.[26] The spectrum changes of CS are more significant. The spectrum shows upshifts in the frequencies of D and G peaks with the additional disorder related peak (D′) observed at 1620 cm^{-1}, originating from the intravalley double resonance.[31] The I_D/I_G ratio of CS decreases to 0.908, which are mostly due to decrease of defect sites (i.e. carbonization of sucrose) by annealing. It is still believed that small amounts of oxygen functional groups exist at the surface of CS. The CSN shows the D and G peaks at ~1364 and ~1600 cm^{-1}, respectively, with the I_D/I_G ratio of 1.13 and it trades off between aMWNT and CS. Together with TEM results, we suspect that the CSN consists of thin CS layer with oxygen-containing functionalities on the conductive MWNT network with a little defects.

The chemical structure is further characterized by X-ray photoelectron spectroscopy (XPS) spectroscopy (Fig. 3b-d). The deconvoluted C1s XPS spectrum of CS presents three peaks assigned to graphitic structure (C-C/C=C) at 284.6 eV, hydroxyl/epoxy groups (C-O) at 286.6 eV, and carbonyl group (O-C=O) at 288 eV. The peaks of C-O and O-C=O are clearly observed that comes from the defects of graphitic carbon layers. For CSN composite, the intensity of oxygen-containing functional groups increases slightly as compared to aMWNT. Particularly, a noticeable increase was made to carbonyl group (i.e. quinone group) at 288 eV which may serve as active site for a reversible redox reaction.[33] These results demonstrate that CS is integrated with MWNT in CSN.

Information on electrochemical performances was collected by cyclic voltammetry (CV) and galvanostatic charge/discharge (GCD) in 1 M Na$_2$SO$_4$ electrolyte and the voltage window of -0.4 to 0.4 V. Fig. 4a represents the CV spectrum of CS at a
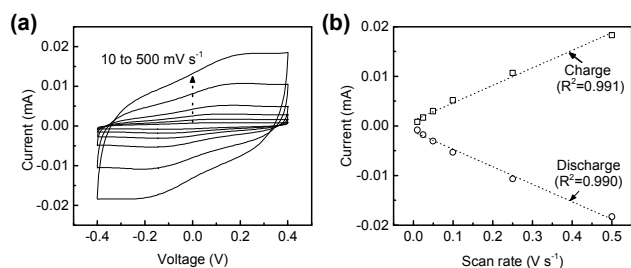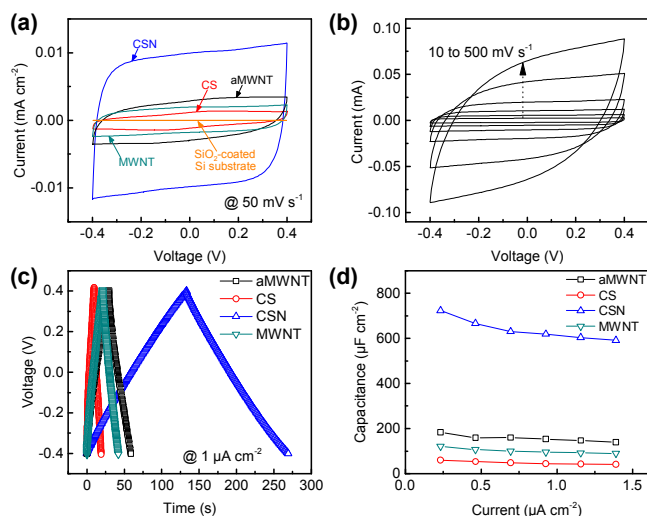

Fig. 5 (a) CV curves of MWNT, aMWNT, CS, and CSN at a scan rate of 50 mV s^{-1}. (b) CV curves of CSN at different scan rate from 10 to 500 mV s^{-1}. (c) GCD curves at a specific current of 1 μA cm^{-2} and (c) rate capability at different currents of MWNT, aMWNT, CS, and CSN.

variety of scan rate ranging from 10 to 500 mV s^{-1}. A reversible redox wave of CS at ~0 V of formal potential was clearly observed.[34, 35] It indicates that redox active surface functional groups are located at the CS surface. Accordingly, these peaks are attributed to the quinone-hydroquinone redox pair of oxidized carbon surface.[35, 36] These anodic and cathodic peaks are not shifted much with increasing the scan rate, proving small internal resistance of electrode.[37] Linear relationship between the peak capacitive current and the scan rate indicates that the redox reaction of CS follows surface-controlled system (Fig. 4b).[38] The CV features were also recorded at a constant scan rate of 50 mV s^{-1} (Fig. 5a). CSN electrode exhibits nearly rectangular CV profiles with symmetric cathodic/anodic currents, which is a typical of ideal SC. Even at fast scan rate of 500 mV s^{-1}, the CV curves almost retain rectangular shapes with little distortion, which is due to low equivalent series resistance (ESR) and fast ion diffusion of the electrode to assure good charge propagation (Fig. 5b).[39] The cathodic/anodic current value of aMWNT is not much different and a little larger than than that of MWNT. Interestingly, the current values of CSN are particularly larger than those of MWNT and CS. This is further corroborated by GCD measurements at a constant current of 1 μA cm^{-2} (Fig. 5c). The GCD curve of CSN exhibits symmetric triangular curves with long duration times and small *IR* drop, confirming an efficient EDL behavior, however, the duration times of MWNT and CS for charging/discharging are much smaller, indicating more resistive behavior.[33] The areal capacitance of CSN is ~615 μF cm^{-2}, larger than ~150 μF cm^{-2} for aMWNT and ~43 μF cm^{-2} for CS. The areal capacitance is comparable to what can be found for literatures.[40, 41] The difference in capacitance values levels out even at high specific current as confirmed by rate capability (Fig. 5d). The initial capacitance of CSN, ~723 μF cm^{-2} measured at 0.23 μA cm^{-2}, remains as high as 591 μF cm^{-2} at a high discharge current of 1.4 μA cm^{-2}, corresponding to 81% retention.

Electrochemical impedance spectroscopy (EIS) was performed by estimating frequency response characteristics over a frequency range of 10^6 to 10^{-2} Hz (Fig. 6). The intercept to the real axis (Z′) of the Nyquist plots represents equivalent

Fig. 4 (a) CV profiles of CS on scan rate ranging from 10 to 500 mV s^{-1}. (b) Plots of scan rate (10 to 500 mV s^{-1}) vs. peak capacitive current for the charge (R^2=0.991) and discharge (R^2=0.990) curves.
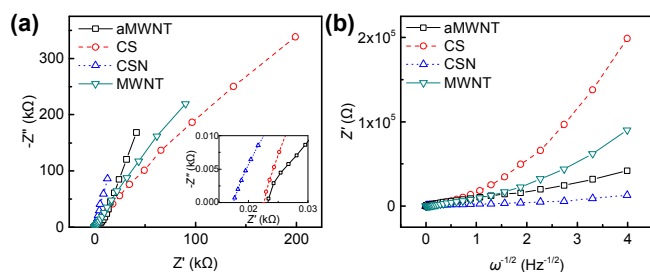
Fig. 6 (a) Nyquist and (b) Randles plots of MWNT, CS, and CSN in the frequency range from 100 kHz to 0.01 Hz measured at equilibrium open circuit potential (~0 V).

series resistance (ESR), involving electrolyte-induced resistance and internal resistance of electrode materials (Fig. 6a).[42] The ESRs are 1.7 Ω for CSN, larger than 2.2 Ω for CS and 2.3 Ω for aMWNT. Since the same electrolyte (1 M Na_2SO_4) was utilized in this study, the change in ESR must result from the electronic and morphological properties of the electrodes. A near vertical curve of CSN has the largest slope with respect to real axis (Z′), demonstrating purely capacitive behavior, while the curves of aMWNT and CS tend to lean toward x-axis, indicating more resistive behavior. It is known that the deviation from the vertical line of the Nyquist plot is credited with inner-pore diffusion limitation by electrolyte ions.[43] Consequently, the unique structure of CSN, CS-deposited MWNT network with macroscopic structure, forms conductive interconnected channels and thus shortens the distances of ion/electron travel.[44, 45] Ion diffusion in the electrode is further proved by the impedance in the medium-low frequency region (1~0.01 Hz). The slope of plot of Z′ against $\omega^{-1/2}$ (so-called Randles plot, Fig. 6b) corresponds to the Warburg coefficient (k_w), which is related to the ion diffusion coefficient (D) as follows:

$$k_w = \frac{RT}{n^2 F^2 A \sqrt{2}} \left(\frac{1}{D^{1/2} C^*} \right)$$

where R is the gas constant, T is the absolute temperature in Kelvin, n is the charge transfer number, A is the area of electrode surface, and C^* is the ionic concentration. The diffusion coefficient of CSN is ~4.88 × 10^{-23} cm^2 s^{-1}, larger than ~2.43 × 10^{-23} and 9.71 × 10^{-23} cm^2 s^{-1} for aMWNT and CS, respectively. We again highlight that the interconnected porous network structure of CSN can form ion-buffering reservoirs, minimizing the ion diffusion distance into inner active sites.[46-48] With spectroscopic and electroanalytic results, we can conclude that the improved capacitance of CSN relative to those of aMWNT and CS can be ascribed to the synergistic effects of i) its high electrical conductivity enhanced by thin CS layers at the outer surface of MWNT as substantiated by ESR, ii) porous architecture due to the network of MWNT bundles that facilitates ion transport, and iii) redox active surface functional groups of CS which contribute to charge accumulation through Faradaic reaction and improve the wettability of carbon materials by aqueous electrolyte, enhancing ion-accessibility to the surface of carbon.[44]

Electrochemical stability of CSN electrode is investigated by performing repeated GCD cycling at 6.7 μA cm^{-2}. CSN electrode preserves over 90% of its initial capacitance for at least 3000 cycles, indicating a good cycle life (Fig. 7).

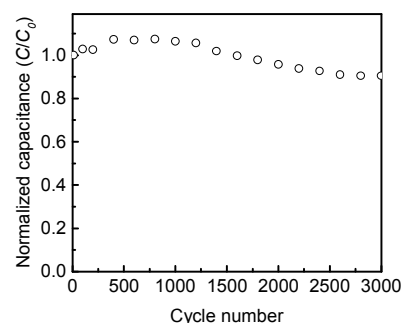**Fig. 7** Cycle stability of CSN electrode at a constant current of 6.7 μA cm^{-2}.

Conclusions

A new composite electrode was fabricated through a simple spin-coating of mixture solution of MWNT and sucrose, followed by thermal treatment at 1000 °C. The CSN forms a continuous conducting network as the sucrose is carbonized and attached onto entangled porous MWNT framework. This unique structure endows the CSN electrode with good areal capacitance (up to 723 μF cm^{-2}) and fast rate capability (~81% retention) greater than the pristine MWNT, aMWNT, and CS due to its high electrical conductivity, porous architecture, and redox behavior. It also exhibits long-term cycle stability for at least 3000 charging/discharging cycles. This nanostructured carbon material show promise as a platform to design high-performance, thin film electrode for energy storages.

Acknowledgements

Notes and references

[a] Department of Materials Science and Engineering, University of Illinois at Urbana-Champaign, Urbana, Illinois, 61801, USA.

[b] School of Chemical Engineering, Sungkyunkwan University (SKKU), Suwon 440-746, Republic of Korea. E-mail:milleniumphs@gmail.com

† Footnotes should appear here. These might include comments relevant to but not central to the matter under discussion, limited experimental and spectral data, and crystallographic data.

Electronic Supplementary Information (ESI) available: [details of any supplementary information available should be included here]. See DOI: 10.1039/b000000x/

1. M. Winter and R. J. Brodd, *Chem. Rev.*, 2004, **104**, 4245-4270.
2. C. Meng, C. Liu, L. Chen, C. Hu and S. Fan, *Nano Lett.*, 2010, **10**, 4025-4031.
3. B. G. Choi, J. Hong, W. H. Hong, P. T. Hammond and H. Park, *ACS Nano*, 2011, **5**, 7205-7213.

4. M. F. El-Kady, V. Strong, S. Dubin and R. B. Kaner, *Science*, 2012, **335**, 1326-1330.

5. W. Gao, N. Singh, L. Song, Z. Liu, A. L. M. Reddy, L. Ci, R. Vajtai, Q. Zhang, B. Wei and P. M. Ajayan, *Nature Nanotech.*, 2011, **6**, 496-500.

6. T. Tomai, S. Mitani, D. Komatsu, Y. Kawaguchi and I. Honma, *Sci. Rep.*, 2014, **4**, 3591.

7. M. Endo, T. Maeda, T. Takeda, Y. J. Kim, K. Koshiba, H. Hara and M. S. Dresselhaus, *J. Electrochem. Soc.*, 2001, **148**, A910-A914.

8. S. Chabi, C. Peng, D. Hu and Y. Zhu, *Adv. Mater.*, 2014, **26**, 2440-2445.

9. D. N. Futaba, K. Hata, T. Yamada, T. Hiraoka, Y. Hayamizu, Y. Kakudate, O. Tanaike, H. Hatori, M. Yumura and S. Iijima, *Nature Mater.*, 2006, **5**, 987-994.

10. J. Chmiola, G. Yushin, Y. Gogotsi, C. Portet, P. Simon and P. L. Taberna, *Science*, 2006, **313**, 1760-1763.

11. J. Chmiola, C. Largeot, P.-L. Taberna, P. Simon and Y. Gogotsi, *Science*, 2010, **328**, 480-483.

12. D. Pech, M. Brunet, H. Durou, P. Huang, V. Mochalin, Y. Gogotsi, P.-L. Taberna and P. Simon, *Nature Nanotech.*, 2010, **5**, 651-654.

13. Z. Niu, J. Chen, H. H. Hng, J. Ma and X. Chen, *Adv. Mater.*, 2012, **24**, 4144-4150.

14. B. E. Conway, *Kluwer Academic/Plenum Publishers, New York*, **1999**.

15. J. Ren, L. Li, C. Chen, X. Chen, Z. Cai, L. Qiu, Y. Wang, X. Zhu and H. Peng, *Adv. Mater.*, 2013, **25**, 1155-1159.

16. H. Jiang, T. Zhao, C. Li and J. Ma, *Chem. Commun.*, 2011, **47**, 8590-8592.

17. Z.-S. Wu, D.-W. Wang, W. Ren, J. Zhao, G. Zhou, F. Li and H.-M. Cheng, *Adv. Funct. Mater.*, 2010, **20**, 3595-3602.

18. M. Beidaghi and C. Wang, *Adv. Funct. Mater.*, 2012, **22**, 4501-4510.

19. J. Lin, C. Zhang, Z. Yan, Y. Zhu, Z. Peng, R. H. Hauge, D. Natelson and J. M. Tour, *Nano Lett.*, 2012, **13**, 72-78.

20. H. R. Byon, S. W. Lee, S. Chen, P. T. Hammond and Y. Shao-Horn, *Carbon*, 2011, **49**, 457-467.

21. W. Chen, R. B. Rakhi, L. Hu, X. Xie, Y. Cui and H. N. Alshareef, *Nano Lett.*, 2011, **11**, 5165-5172.

22. Y. Luo, X. Xu, Y. Zhang, Y. Pi, Y. Zhao, X. Tian, Q. An, Q. Wei and L. Mai, *Adv. Energy Mater.*, DOI: 10.1002/aenm.201400107.

23. H. Mi, X. Zhang, S. An, X. Ye and S. Yang, *Electrochem. Commun.*, 2007, **9**, 2859-2862.

24. K. Böhme, W.-D. Einicke and O. Klepel, *Carbon*, 2005, **43**, 1918-1925.

25. J. Ren, W. Bai, G. Guan, Y. Zhang and H. Peng, *Adv. Mater.*, 2013, **25**, 5965-5970.

26. M. Armandi, B. Bonelli, F. Geobaldo and E. Garrone, *Microporous Mesoporous Mater.*, 2010, **132**, 414-420.

27. L. He, M. Toda, Y. Kawai, H. Miyashita, M. Omori, T. Hashida, R. Berger and T. Ono, *Microsys. Technol.*, 2014, **20**, 201-208.

28. P. C. Eklund, J. M. Holden and R. A. Jishi, *Carbon*, 1995, **33**, 959-972.

29. K. Dong Chul, J. Dae-Young, C. Hyun-Jong, W. YunSung, S. Jai Kwang and S. Sunae, *Nanotechnology*, 2009, **20**, 375703.

30. D. Yuan, X. Yuan, W. Zou, F. Zeng, X. Huang and S. Zhou, *J. Mater. Chem.*, 2012, **22**, 17820-17826.

31. J. Hong, M. K. Park, E. J. Lee, D. Lee, D. S. Hwang and S. Ryu, *Sci. Rep.*, 2013, **3**, 2700.

32. H. Wang, Q. Hao, X. Yang, L. Lu and X. Wang, *Nanoscale*, 2010, **2**, 2164-2170.

33. S.-K. Kim, Y. K. Kim, H. Lee, S. B. Lee and H. S. Park, *ChemSusChem*, 2014, **7**, 1094-1101.

34. E. Raymundo-Piñero, F. Leroux and F. Béguin, *Adv. Mater.*, 2006, **18**, 1877-1882.

35. K. T. Lee, X. Ji, M. Rault and L. F. Nazar, *Angew. Chem. Int. Ed.*, 2009, **48**, 5661-5665.

36. S. Biniak, A. Swiatkowski and M. Makula, **2001, Ch. 3.**

37. H. B. Li, M. H. Yu, F. X. Wang, P. Liu, Y. Liang, J. Xiao, C. X. Wang, Y. X. Tong and G. W. Yang, *Nat. Commun.*, 2013, **4**, 1894.

38. M. D. Stoller, S. Park, Y. Zhu, J. An and R. S. Ruoff, *Nano Lett.*, 2008, **8**, 3498-3502.

39. S. Bose, T. Kuila, A. K. Mishra, R. Rajasekar, N. H. Kim and J. H. Lee, *J. Mater. Chem.*, 2012, **22**, 767-784.

40. H. Y. Jung, M. B. Karimi, M. G. Hahm, P. M. Ajayan and Y. J. Jung, *Sci. Rep.*, 2012, **2**, 773.

41. G. Zheng, L. Hu, H. Wu, X. Xie and Y. Cui, *Energy Environ. Sci.*, 2011, **4**, 3368-3373.

42. M. D. Stoller and R. S. Ruoff, *Energy Environ. Sci.*, 2010, **3**, 1294-1301.

43. D.-W. Wang, F. Li, H.-T. Fang, M. Liu, G.-Q. Lu and H.-M. Cheng, *J. Phys. Chem. B*, 2006, **110**, 8570-8575.

44. Z.-L. Wang, D. Xu, H.-G. Wang, Z. Wu and X.-B. Zhang, *ACS Nano*, 2013, **7**, 2422-2430.

45. X. Yang, J. Zhu, L. Qiu and D. Li, *Adv. Mater.*, 2011, **23**, 2833-2838.

46. L. Z. Fan, Y. S. Hu, J. Maier, P. Adelhelm, B. Smarsly and M. Antonietti, *Adv. Funct. Mater.*, 2007, **17**, 3083-3087.

47. J. Chen and K. Yano, *ACS Appl. Mater. Interfaces*, 2013, **5**, 7682-7687.

48. G.-J. Lee and S.-I. Pyun, *Langmuir*, 2006, **22**, 10659-10665.

Table of contents

Sucrose-derived thin carbon layer (CS) is coated on the surface of multiwalled carbon nanotube (MWNT) and the resulting composite electrode (CSN) provides larger capacitance than that of MWNT and CS.

RSC Advances Accepted Manuscript